Isotopic effects in sub-barrier fusion of Si + Si systems

G. Colucci,[1] G. Montagnoli,[1] A. M. Stefanini,[2] H. Esbensen,[3] D. Bourgin,[4] P. Čolović,[5] L. Corradi,[2] M. Faggian,[1,*] E. Fioretto,[2] F. Galtarossa,[2,6] A. Goasduff,[1] J. Grebosz,[7] F. Haas,[4] M. Mazzocco,[1] F. Scarlassara,[1] C. Stefanini,[1] E. Strano,[1] S. Szilner,[5] M. Urbani,[1,†] and G. L. Zhang[1,8]

[1]*Dipartimento di Fisica e Astronomia, Università di Padova, and INFN, Sezione di Padova, I-35131 Padova, Italy*
[2]*INFN, Laboratori Nazionali di Legnaro, I-35020 Legnaro (Padova), Italy*
[3]*Physics Division, Argonne National Laboratory, Argonne, Illinois 60439, USA*
[4]*IPHC, CNRS-IN2P3, Université de Strasbourg, F-67037 Strasbourg Cedex 2, France*
[5]*Ruđer Bošković Institute, HR-10002 Zagreb, Croatia*
[6]*Dipartimento di Fisica e Scienze della Terra, Universitá di Ferrara, I-44121 Ferrara, Italy*
[7]*Institute of Nuclear Physics, Polish Academy of Sciences, PL 31-342 Cracow, Poland*
[8]*School of Physics and Nuclear Energy Engineering, Beihang University, Beijing 100191, China*

(Received 23 January 2018; published 23 April 2018)

Background: Recent measurements of fusion cross sections for the $^{28}\mathrm{Si} + ^{28}\mathrm{Si}$ system revealed a rather unsystematic behavior; i.e., they drop faster near the barrier than at lower energies. This was tentatively attributed to the large oblate deformation of ^{28}Si because coupled-channels (CC) calculations largely underestimate the $^{28}\mathrm{Si} + ^{28}\mathrm{Si}$ cross sections at low energies, unless a weak imaginary potential is applied, probably simulating the deformation. ^{30}Si has no permanent deformation and its low-energy excitations are of a vibrational nature. Previous measurements of this system reached only 4 mb, which is not sufficient to obtain information on effects that should show up at lower energies.

Purpose: The aim of the present experiment was twofold: (i) to clarify the underlying fusion dynamics by measuring the symmetric case $^{30}\mathrm{Si} + ^{30}\mathrm{Si}$ in an energy range from around the Coulomb barrier to deep sub-barrier energies, and (ii) to compare the results with the behavior of $^{28}\mathrm{Si} + ^{28}\mathrm{Si}$ involving two deformed nuclei.

Methods: ^{30}Si beams from the XTU tandem accelerator of the Laboratori Nazionali di Legnaro of the Istituto Nazionale di Fisica Nucleare were used, bombarding thin metallic ^{30}Si targets (50 μg/cm^2) enriched to 99.64% in mass 30. An electrostatic beam deflector allowed the detection of fusion evaporation residues (ERs) at very forward angles, and angular distributions of ERs were measured.

Results: The excitation function of $^{30}\mathrm{Si} + ^{30}\mathrm{Si}$ was measured down to the level of a few microbarns. It has a regular shape, at variance with the unusual trend of $^{28}\mathrm{Si} + ^{28}\mathrm{Si}$. The extracted logarithmic derivative does not reach the L_{CS} limit at low energies, so that no maximum of the S factor shows up. CC calculations were performed including the low-lying 2^+ and 3^- excitations.

Conclusions: Using a Woods-Saxon potential the experimental cross sections at low energies are overpredicted, and this is a clear sign of hindrance, while the calculations performed with a M3Y + repulsion potential nicely fit the data at low energies, without the need of an imaginary potential. The comparison with the results for $^{28}\mathrm{Si} + ^{28}\mathrm{Si}$ strengthens the explanation of the oblate shape of ^{28}Si being the reason for the irregular behavior of that system.

DOI: 10.1103/PhysRevC.97.044613

I. INTRODUCTION

The comparison of fusion data for neighboring systems is a sensitive tool to evidence the influence of nuclear structure on reaction dynamics at energies near and below the Coulomb barrier. A comparative study was recently performed for the Si + Si systems [1], where the interest originated from the different shape of the silicon isotopes. Indeed, ^{28}Si is strongly deformed with an oblate shape while ^{30}Si is nearly spherical. In that work the fusion of the asymmetric system $^{28}\mathrm{Si} + ^{30}\mathrm{Si}$ [1,2] was explained by considering one-neutron and successive two-neutron transfer channels in the coupling scheme. The case of $^{28}\mathrm{Si} + ^{28}\mathrm{Si}$ involving deformed nuclei shows an unusual behavior, where the cross section is hindered [3] just below the barrier and then enhanced at lower energies, as shown in the comparison with the coupled-channels (CC) calculations. It was further surprising that the low-energy data were well reproduced only by artificially applying a weak, short-ranged imaginary potential, probably simulating the effect of the oblate deformation.

*Present address: SUPA, Physics Department and Institute for Complex Systems and Mathematical Biology, King's College, University of Aberdeen, AB24 3UE, UK.

†Present address: Department of Electrical Engineering, Universitat Politècnica de Catalunya, BarcelonaTech (UPC), Terrassa (Barcelona), Spain.

The nucleus ^{30}Si has a spherical shape, because the measured quadrupole moment of the 2^+ state, $Q_2 = -0.05(6)$ barn, is consistent with zero [4]. An attractive comparison could therefore be done between ^{30}Si + ^{30}Si and ^{28}Si + ^{28}Si because no transfer channels with positive Q values exist for both cases. However, the excitation function of ^{30}Si + ^{30}Si was measured only down to $\simeq$4 mb [5], and this prevents a meaningful comparison between the two systems. A further point of interest is the possible appearance of the hindrance phenomenon in this system which has a positive Q value for fusion (+15.6 MeV) that is similar to the case of ^{28}Si + ^{30}Si (14.3 MeV) where an S-factor maximum has almost been reached at the lowest experimental energy (see Fig. 3 of Ref. [2]). Therefore, a fusion experiment has been recently carried out at the Laboratori Nazionali di Legnaro (LNL) with the purpose to extend the data of ^{30}Si + ^{30}Si down to energies deeply below the Coulomb barrier.

Preliminarily data have already been presented at international conferences [6,7]. In this work we present the results of the full measurement, from well below to well above the Coulomb barrier. Section II describes the experimental setup and the analysis procedure, while the results of CC calculations are presented in Sec. III. A comparison with the nearby system ^{28}Si + ^{28}Si follows in Sec. III B. The work is summarized and concluded in Sec. IV.

II. EXPERIMENTAL SETUP AND RESULTS

Beams of ^{30}Si in the energy range of 47–90 MeV, with intensities of 15–30 pnA, were provided by the XTU tandem accelerator of the LNL of the Istituto Nazionale di Fisica Nucleare (INFN). The targets consisted of 50 μg/cm^2 ^{30}Si evaporated on 30 μg/cm^2 carbon backings facing the beam. The isotopic enrichment of ^{30}Si was 99.64%. The fusion yields were not essentially affected by the small residual contaminations of ^{29}Si and ^{28}Si because of their higher Coulomb barriers with respect to ^{30}Si. The carbon backing and the silicon target itself introduced an average beam energy loss of around 750–850 keV, which was taken into account in the analysis.

Fusion cross sections have been determined by direct detection of the fusion evaporation residues (ERs) at small angles by separating out the beam and beamlike particles using the electrostatic beam deflector of the LNL, which allows fast and reliable measurements of relative and absolute cross sections [1,8]. The ERs were identified downstream of the deflector by a double time-of-flight (ToF) ΔE-energy telescope composed of two microchannel plate time detectors followed by a transverse-field ionization chamber (IC) and by a silicon detector placed in the same gas (CH_4) volume of the IC. The silicon detector measured the residual energy of the ERs and gave the start signal for the two ToF telescopes as well as the trigger for the data acquisition. We report in Fig. 1 representative examples of two-dimensional plots of ΔE-ToF where ERs can be easily recognized both near and much below the Coulomb barrier. These spectra were collected in 20 min and in 8 h of beam time, respectively, with comparable beam intensities.

A good separation of ER events from the residual beamlike particles is achieved at energies both above and below the Coulomb barrier. Four silicon detectors were placed symmetrically around the beam direction at the same scattering angle $\theta_{\rm lab} = 16^\circ$, used to monitor the beam and to normalize the fusion yields to the Mott scattering cross section. Three ER angular distributions were measured at the energies of 58, 72, and 80 MeV in the range from -6° to $+9^\circ$. We observed that their shape does not appreciably change with energy, in agreement with several other cases that have been studied in the past (see, e.g., Refs. [9,10]). This enables the ratio of the differential cross section to the total fusion cross section to be accurately estimated at any energy; therefore we could obtain total fusion cross sections by integrating those distributions and by simple interpolations or extrapolations for all other energies where ER measurements were taken only at 2° (or 3° for low energies). The error on the cross sections for the energies where no angular distribution was measured is not essentially increased by this procedure. We point out that the statistical uncertainty is anyway dominant from the barrier down, which is the range of energies relevant for the physical issues investigated in this work.

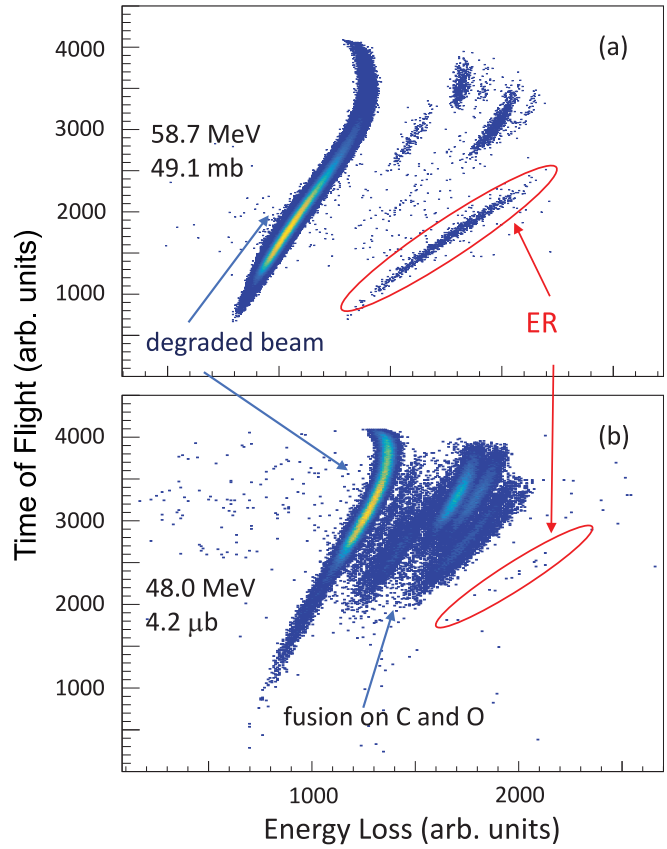

FIG. 1. Two-dimensional spectra of time of flight vs energy loss measured at different beam energies around (a) and far below the Coulomb barrier (b), for ^{30}Si + ^{30}Si. The nominal beam energies and the corresponding fusion cross sections are reported. The detected events within the oval shapes are identified as fusion evaporation residues (ER) and are indicated by the red arrows. They are well separated from the other kinds of events due to degraded beam and to fusion on carbon and oxygen present in the target.

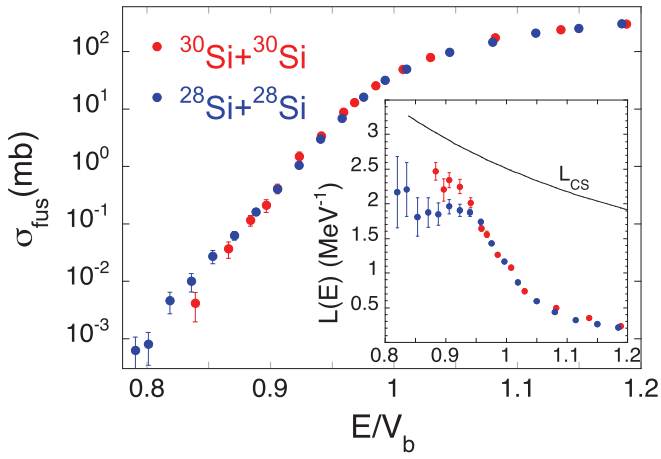

FIG. 2. Fusion excitation function of ^{30}Si + ^{30}Si measured in this work, compared to the system ^{28}Si + ^{28}Si [1]. The energy scale is normalized to the Akyüz-Winther Coulomb barrier [11]. The reported errors are purely statistical uncertainties. The insert shows the logarithmic derivatives (slopes) of the excitation functions for the two systems.

The absolute cross section scale may be fixed, as in previous experiments using the same setup, by knowledge of the relevant detector solid angles and of the deflector transmission and by the angular distribution integrations. Overall, the uncertainties affecting these quantities normally introduce a ±7–8% error in that absolute scale. In the present case, however, the silicon detector at the end of the telescope had to be replaced during the measurements with a new one having a different active area, due to an unexpected failure of the old one. This introduced a not negligible additional uncertainty (probably ≃10%) in the derivation of the absolute fusion cross sections. Therefore, we found it more reliable to normalize the present data to the previous results of Bozek *et al.* [5] above the barrier. All cross sections, logarithmic derivatives, and S factors reported in the remainder of this article derive from the normalization of the scale we decided to perform at $E_{\text{c.m.}} = 34.9$ MeV, because this energy is common to the present experiment and the previous experiments. At this energy the cross section quoted in Ref. [5] is 469 ± 60 mb, so that the absolute cross section scale in the present work is affected by the same uncertainty (±13%). However, only statistical errors influence the relative cross sections.

The full set of fusion cross sections measured for ^{30}Si + ^{30}Si in this work are reported in Fig. 2, where we noticed that the excitation function has been extended down to ≃4 μb. In the same figure a comparison is done with the existing excitation function of ^{28}Si + ^{28}Si [1] in a reduced energy scale. The two excitation functions appear to have different trends below the barrier. Indeed, as anticipated in the Introduction, the cross sections of the lighter system drop faster just below the barrier than at lower energies. On the contrary, the excitation function measured for ^{30}Si + ^{30}Si in the present work has a smoother behavior in the whole sub-barrier energy range.

The insert in Fig. 2 shows the logarithmic derivatives (slopes) of the excitation functions for the two systems. In either case, the slopes do not cross the L_{CS} value expected for a constant astrophysical S factor. This would phenomenologically suggest the absence of hindrance [3] in the measured energy range, and this was claimed in the analysis of Ref. [7]. However a comparison with full CC calculations is necessary to confirm or disprove that evidence. This was already performed for ^{28}Si + ^{28}Si in Refs. [1,12] and the following section shows the results of analogous calculations for ^{30}Si + ^{30}Si.

TABLE I. Results of the analysis of the present ^{30}Si + ^{30}Si fusion data. The Ch-10w5 and Ch-15w5 calculations include 10 and 15 channels, respectively, and an imaginary potential with depth $w = -5$ MeV, radius $R_w = 6.63$ fm, and diffuseness $a_w = 0.2$ fm. A systematic error of 5% was adopted in the analysis. The radius R of the neutron density was adjusted in each case to minimize the χ^2, whereas the charge radius was kept fixed at 3.165 fm (see Table II). The minimum of the pocket, V_{min}, and the height of the Coulomb barrier, V_{CB}, are also shown. Similar results are shown for ^{28}Si + ^{28}Si [1,12].

Reaction	a_w (fm)	R (fm)	V_{min}	V_{CB}	χ^2/N
^{30}Si + ^{30}Si Ch-10w5	0.2	3.35	19.52	28.42	0.87
^{30}Si + ^{30}Si Ch-15w5	0.2	3.30	18.85	28.51	0.40
^{28}Si + ^{28}Si Ch-10w5 [1]	0.2	3.135	23.76	29.37	1.71
^{28}Si + ^{28}Si Ch-10w5 [12]	0.3	3.125	23.59	29.41	1.16

III. RESULTS OF COUPLED-CHANNELS CALCULATIONS

A. The system ^{30}Si + ^{30}Si

We have performed CC calculations for ^{30}Si + ^{30}Si using the M3Y + repulsion potential that was introduced in Ref. [13]. The nuclear structure information on the low-lying 2^+ and 3^- states was listed in Table I of Ref. [1]. If we include all of the one- and two-phonon excitations as well as mutual excitations that can be generated by those states, we obtain a total of 15 channels (including the elastic channel). Such calculations are referred to as Ch-15 calculations and are discussed later on.

The two-phonon excitations of the 3^- states have an energy that is larger than 9–10 MeV. If we exclude them, the number of channels is reduced to 12. If we also exclude the mutual excitation of the 2^+ and 3^- states in the same nucleus, the total number of channels is reduced to 10. We have performed such Ch-10 calculations in a previous work [1] where we compared them to the existing data for ^{28}Si + ^{28}Si [1] and ^{30}Si + ^{30}Si [5]. We have repeated them here in an analysis of the present new data for ^{30}Si + ^{30}Si.

Because ^{30}Si is spherical, the CC calculations for ^{30}Si + ^{30}Si are more robust than those for ^{28}Si + ^{28}Si because the location of the minimum of the potential pocket is essentially the same in all reaction channels. One can therefore impose the ingoing-wave boundary conditions for fusion at one common pocket minimum. This is not so easy for ^{28}Si + ^{28}Si because the pocket minima are located at different radial separations. The problem was solved in Refs. [1,12] by applying an imaginary potential with a diffuseness of $a_w = 0.2$ to 0.3 fm.

However, it turns out (as is often the case see, e.g., Fig. 11 of Ref. [14]) that we need a short-ranged imaginary potential to explain the data at high energies. The Ch-10w5 and

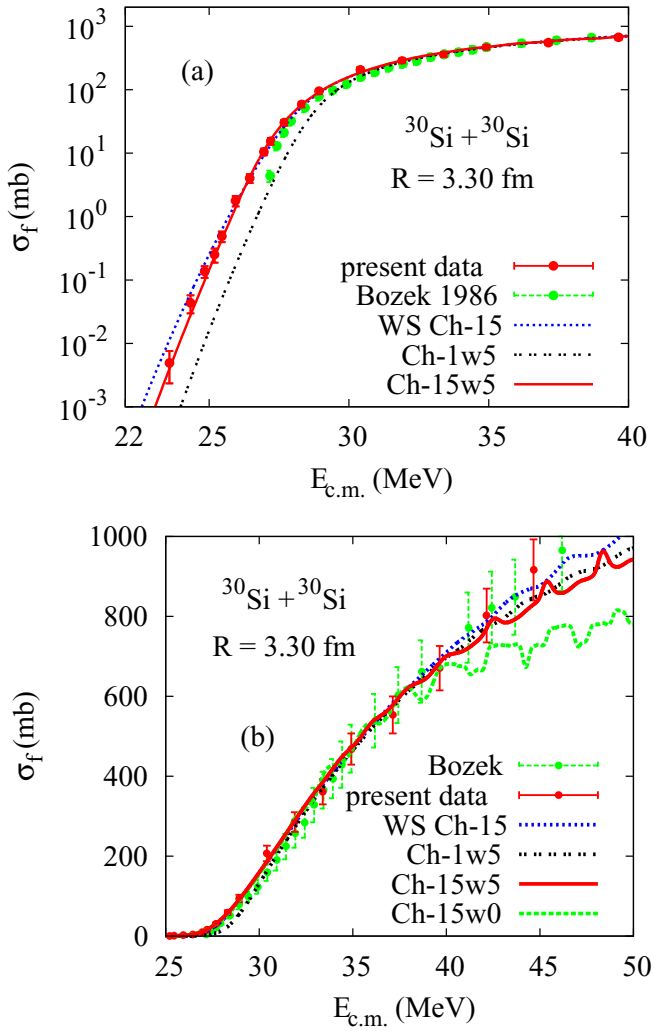

FIG. 3. Logarithmic (a) and linear plot (b) of the present and previously measured (Bozek *et al.* [5]) fusion cross sections for ^{30}Si + ^{30}Si. The data are compared to Ch-1 and Ch-15 CC calculations that are based on the M3Y + repulsion potential with parameters $a_r = 0.38$ fm and radius $R = 3.30$ fm of the neutron density. Also shown are the results of Ch-15 calculations that use a Woods-Saxon (WS) potential with parameters $R = 7.177$ fm, $U_0 = -55.37$ MeV, and $a = 0.637$ fm. The radius R was adjusted to reproduce the data at energies above the Coulomb barrier. The calculation Ch-15w0 shown in panel (b) illustrates the importance of an imaginary potential at high energies.

Ch-15w5 calculations include such a weak imaginary potential, parametrized as a simple Woods-Saxon well with depth $w_0 = -5$ MeV, radius $R_w = 6.63$ fm, and diffuseness $a_w = 0.2$ fm. The results of the best Ch-15w5 calculations are compared with the data in Fig. 3. It is seen in Fig. 3(b) that the calculations reproduce the high-energy data much better than the Ch-15w0 calculations that do not include any imaginary potential. No-coupling calculations (Ch-1w5) are also reported in Fig. 3.

The present ^{30}Si + ^{30}Si data are analyzed in terms of the χ^2 per data point (χ^2/N). The best fit to the data in each set of calculations is obtained by adjusting the radius of the

TABLE II. Radius R and diffuseness a of the proton and neutron densities in ^{28}Si and ^{30}Si. The proton densities (the first and fourth lines) were adjusted to reproduce the known point-proton rms radii [15]. The proton + neutron densities were used to calculate the M3Y + repulsion potential [13]. The radii of the neutron density of ^{30}Si shown in lines 2 and 3 were obtained by optimizing the fit to the present ^{30}Si + ^{30}Si fusion data in Ch-10w5 and Ch-15w5 calculations, respectively. Similar results were obtained for ^{28}Si in Refs. [1,12] from the analysis of the ^{28}Si + ^{28}Si fusion data. The parameter a_w is the adopted diffuseness of the imaginary potential.

Source	a_w (fm)	R (fm)	a (fm)	rms	rms (pp)	rms (ch)
^{30}Si [15]		3.165	0.48	3.032	3.032(4)	3.133(4)
Ch-10w5	0.2	3.35	0.48	3.149	Fusion	New data
Ch-15w5	0.2	3.30	0.48	3.117	Fusion	New data
^{28}Si [15]		3.141	0.48	3.018	3.018(2)	3.122(2)
Ch-10w5	0.2	3.135	0.48	3.013	Fusion	Ref. [1]
Ch-10w5	0.3	3.125	0.48	3.007	Fusion	Ref. [12]

neutron density that is used to calculate the M3Y + repulsion double-folding potential. The proton density, on the other hand, is kept fixed with the radius $R = 3.165$ fm and the diffuseness $a = 0.48$ fm. These values are consistent with the experimental point-proton rms radius of ^{30}Si (see the first line of Table II). In general, the point-proton density is very well established by the measured rms charge radius, whereas the point-neutron density is more uncertain. It is therefore natural to adopt the known point-proton density, whereas the point-neutron density can be determined by optimizing the fit to the fusion data.

The diffuseness of the density associated with the repulsive part of the M3Y + repulsion interaction was set to $a_r = 0.38$ fm. The Ch-15w5 calculations are smoother and rise more steeply at high energies than the Ch-15w0 calculations where no imaginary potential is applied. This can be seen in Fig. 3(b). The calculations that include absorption do exhibit some structures at high energies. These structures can be associated with the individual centrifugal barriers that we discussed in previous works [12,14].

The results of the analysis that is based on Ch-10w5 and Ch-15w5 calculations, respectively, are shown in lines 1 and 2 of Table I. The results were obtained by minimizing the χ^2/N for each set of calculations with respect to the radius R of the neutron density. The radial dependence of the χ^2/N values that were used to determine the best fits in Ch-10w5 and Ch-15w5 calculations are illustrated in Fig. 4.

It is interesting to note that the adjusted value of the neutron density radius obtained in Ch-15w5 is smaller than that in Ch-10w5 calculations. The difference is of the order of 0.05 fm. The reason for this is that the smaller radius obtained in Ch-15 calculations is compensated by the polarization of high-lying states that are included in Ch-15 calculations but not in Ch-10 calculations.

Another observation in Table I is that the χ^2/N is much improved in the Ch-15w5 calculations compared to the result of the Ch-10w5 analysis. The reason is that the enhancement of sub-barrier fusion is larger in Ch-15 calculations than in Ch-10 calculations, and such an enhancement is evidently preferred by the data. We therefore only show the results of Ch-15w5

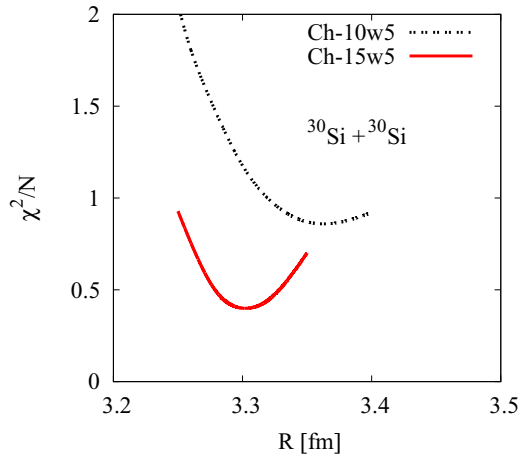

FIG. 4. χ^2 analysis of the present data by Ch-10w5 and Ch-15w5 calculations, respectively, as functions of the radius R of the neutron density in ^{30}Si. The data have been normalized to the data of Bozek *et al.* [5] at 34.9 MeV.

calculations in the following. By the comparison of the best fit with the data in Fig. 3, it is seen that the Ch-15w5 results are in excellent agreement with the data.

The analogous Ch-15 results using a standard Woods-Saxon (WS) potential are also shown in Fig. 3. The radius of the potential, $R = 7.177$ fm, was adjusted so that the data were reproduced at energies above the Coulomb barrier. It is seen that the data are suppressed compared to this calculation at the lowest energies, which is a sign of the fusion hindrance phenomenon [3]. The suppression is evidently removed by applying the adjusted M3Y + repulsion potential as illustrated in Fig. 3(a).

B. Comparison of results for the two systems

The analysis of the ^{28}Si + ^{28}Si fusion data [1] that was performed in Refs. [1,12] was based on Ch-10 calculations. The results are listed in lines 3 and 4 of Table I. It was found that the fit to the data could be improved by increasing the diffuseness a_w of the imaginary potential, from 0.2 to 0.3 fm. The need for a larger diffuseness was justified by the large deformation of ^{28}Si (see Ref. [1] for details). We therefore in the following show the results of these calculations that are denoted Ch-10aw3w5.

The excitation functions for ^{28}Si + ^{28}Si and ^{30}Si + ^{30}Si are compared in Fig. 5. The best fit to the ^{28}Si + ^{28}Si data was obtained in Ch-10aw3w5 calculations and is seen to be in excellent agreement with the data at all energies. The calculation Ch-10w0 that does not include any imaginary potential is also shown in Fig. 5(a), and it is seen to underpredict the data substantially at low energies.

We showed in Ref. [12] that the structures in the high-energy fusion of ^{28}Si + ^{28}Si are strongly influenced by coupled-channels effects. On the other hand, the structures are much weaker in the no-coupling calculations. Because the couplings (both quadrupole and octupole) are much weaker in the ^{30}Si + ^{30}Si reaction (see Table I of Ref. [1]), it is therefore not

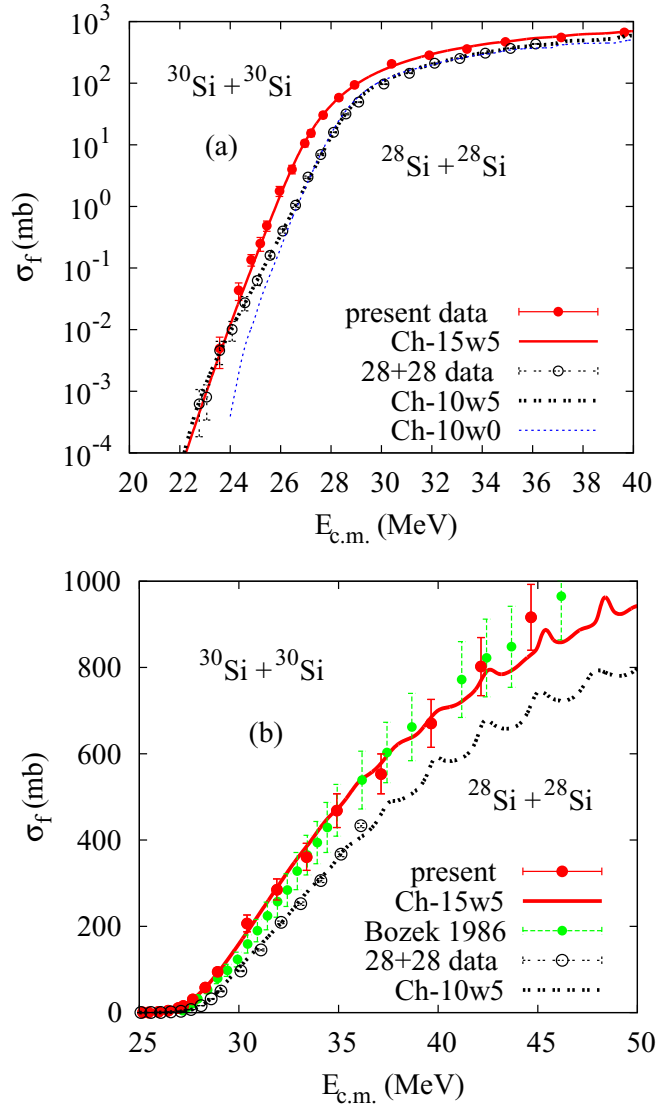

FIG. 5. Logarithmic (a) and linear (b) plots of the best fits to the ^{28}Si + ^{28}Si fusion data [1] and the present ^{30}Si + ^{30}Si fusion data obtained with Ch-10w5 and Ch-15w5 calculations, respectively.

surprising that the structures shown in Fig. 5(b) are different and even weaker in the fusion of ^{30}Si + ^{30}Si.

A detailed comparison of the S factors for fusion and the logarithmic derivatives of both systems is shown in Fig. 6. We point out that the logarithmic derivative is insensitive to the absolute normalization of the cross section. The good agreement between the best calculation and the data shows that the shape of the calculated excitation function is consistent with the shape of the measured cross sections.

Another interesting feature observed in Fig. 6 is that the calculations Ch-15w0 and Ch-15w5 are both in good agreement with the data for ^{30}Si + ^{30}Si at low energies (see the right panels), whereas the Ch-10-w0 and Ch-10w5 calculations for ^{28}Si + ^{28}Si (left panels) differ substantially from each other at the lowest energies and only the Ch-10aw3w5 calculation is able to reproduce the data. These features are consistent with the spherical nature of ^{30}Si and the deformation of ^{28}Si.

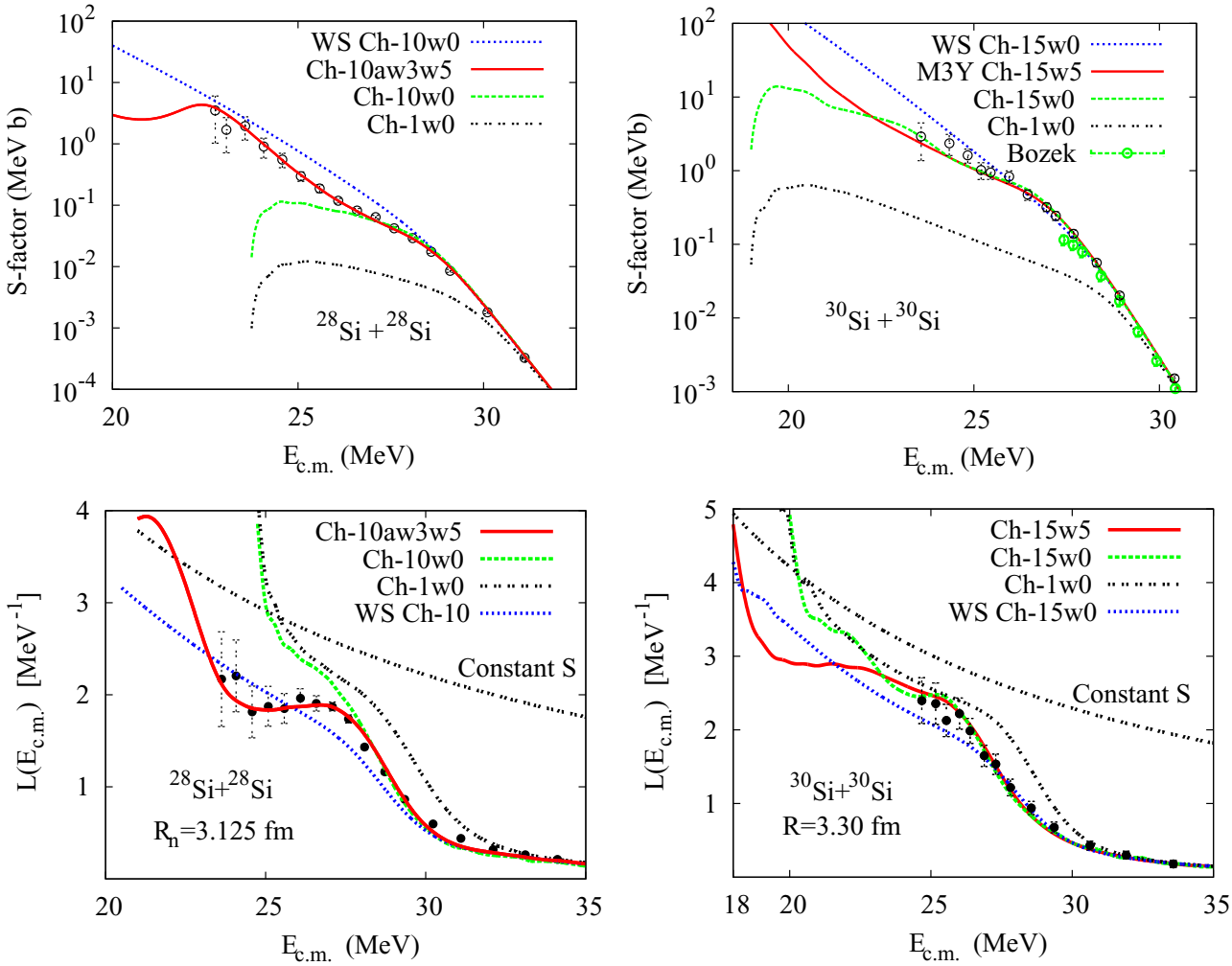

FIG. 6. *S* factors (upper panels) and logarithmic slopes of the excitation functions (lower panels) for the fusion of ^{28}Si + ^{28}Si [1] and ^{30}Si + ^{30}Si (see also Ref. [5]) are compared to the best Ch-10 and Ch-15 calculations, respectively, with (w5) and without (w0) an imaginary potential. Ch-1w0 calculations (no coupling results) are reported for reference. Results that are based on a WS potential (adjusted to reproduce the high-energy data) are also shown.

Indeed, the deformation of ^{28}Si produces barriers at different radial separations in the excited channels, as discussed in Ref. [1]. Those calculations were performed by imposing the ingoing-wave boundary conditions at the barrier of the elastic channel but the imaginary potential made it possible to probe the barriers that were located at different separations. The barriers in Fig. 4(b) of Ref. [1] associated with the excitations of the spherical nucleus ^{30}Si, on the other hand, are located essentially at the same radial separation, and a weak imaginary potential was therefore not expected to have an effect. It does have some influence as illustrated in Fig. 6 but the difference sets in at much lower energies.

The first derivatives of the energy-weighted cross sections are shown in Fig. 7. The structures observed in the fusion of ^{28}Si + ^{28}Si are associated with the centrifugal barriers in the entrance channel potential, although CC effects do smear out the correlation between a particular barrier and a peak in the first derivative of the energy-weighted cross sections as discussed in Ref. [12]. It is seen that the calculated structures for ^{30}Si + ^{30}Si are weaker, so the possibility of observing these structures experimentally is not so promising.

Figure 8 reports the ratio of the measured and the calculated cross sections that are shown in Fig. 5. Also shown are the ratios of the data to the calculations that are based on a WS potential. It is seen that the ^{28}Si + ^{28}Si data are suppressed or hindered at energies that are slightly below the Coulomb barrier compared to the Ch-10 calculation that uses a WS potential. However, the hindrance disappears at the lowest energies. This unusual behavior is ascribed to the large deformation of ^{28}Si. The data can evidently be reproduced as discussed in Ref. [12] by using the M3Y + repulsion potential and an imaginary potential with the diffuseness $a_w = 0.3$ fm.

On the contrary, it appears from Fig. 8 that the data for ^{30}Si + ^{30}Si agree with the WS calculation slightly below the barrier and become suppressed only at the lowest energies. This is the "normal" evidence of the fusion hindrance phenomenon that was first introduced in Ref. [3].

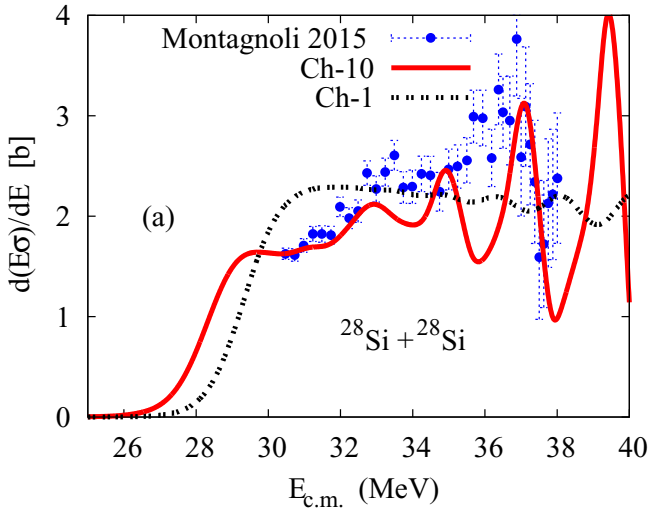

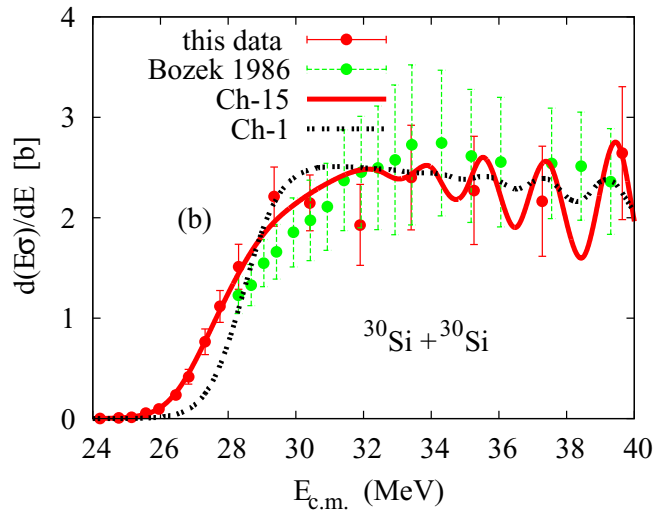

FIG. 7. The first derivative of the energy-weighted cross section for the fusion of ^{28}Si + ^{28}Si (Montagnoli *et al.* [12]) (a) and ^{30}Si + ^{30}Si (b) (present data and Ref. [5]) are compared to the best Ch-10aw3w5 and Ch-15w5 calculations, respectively. The results of Ch-1 calculations are also shown.

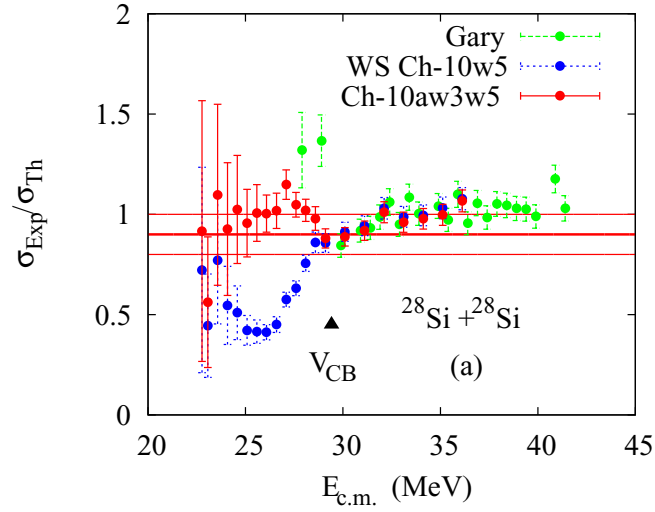

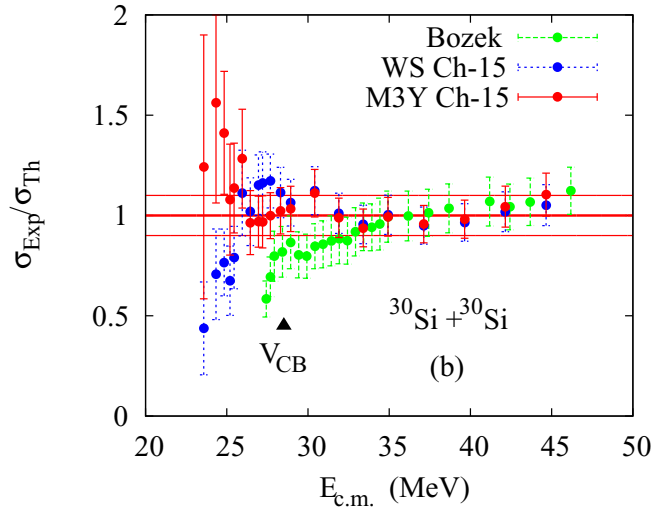

FIG. 8. Ratio of the measured and the calculated cross sections shown in Fig. 5(b) for ^{28}Si + ^{28}Si (a) and ^{30}Si + ^{30}Si (b). The ratio to the WS calculations indicates a fusion hindrance just below the Coulomb barrier for ^{28}Si + ^{28}Si, but that effect is seen to disappear at lower energies (the older data of Gary and Volant are from Ref. [16]). For ^{30}Si + ^{30}Si a fusion hindrance appears at the lowest measured energies.

IV. SUMMARY

The excitation function of ^{30}Si + ^{30}Si has been measured down to the level of a few microbarns using the ^{30}Si beams from the XTU tandem accelerator of the INFN-LNL and an experimental setup with an electrostatic beam deflector, allowing us to detect the ERs at small angles. The excitation function displays a regular behavior, at variance with the unusual trend of the nearby case ^{28}Si + ^{28}Si. The extracted logarithmic derivative does not reach the L_{CS} limit at low energies, so the experimental S factor does not reach a maximum.

Coupled-channels calculations were performed taking into account the one- and two-phonon excitations as well as the mutual excitations of the low-lying 2^+ and 3^- states in projectiles and targets. Using a Woods-Saxon potential the experimental cross sections were overpredicted at low energies, so that we have evidence of the hindrance effect. The analogous calculations performed with a M3Y + repulsion potential reproduced the excitation function very well, in its whole measured energy range. A weak imaginary potential was necessary to fit the high-energy cross sections, but not below the barrier because it was needed for ^{28}Si + ^{28}Si where the hindrance, observed just below the barrier, disappeared at the lowest energies. This was ascribed to the large oblate deformation of ^{28}Si, and this interpretation is reinforced by the different behavior of the symmetric system involving ^{30}Si, which is a spherical nucleus.

ACKNOWLEDGMENTS

We are very grateful to the XTU Tandem staff and to M. Loriggiola for preparing targets of excellent quality. The research leading to these results has received funding from the

European Union Seventh Framework Programme FP7/2007-2013 under Grant No. 262010-ENSAR. This work has been supported in part by the Croatian Science Foundation under Project No. 7194. H.E. is supported by the U.S. Department of Energy, Office of Science, Office of Nuclear Physics, under Contract No. DE-AC02-06CH11357.

[1] G. Montagnoli, A. M. Stefanini, H. Esbensen, C. L. Jiang, L. Corradi, S. Courtin, E. Fioretto, J. Grebosz, F. Haas, H. M. Jia, M. Mazzocco, C. Michelagnoli, T. Mijatović, D. Montanari, C. Parascandolo, F. Scarlassara, E. Strano, S. Szilner, and D. Torresi, Phys. Rev. C **90**, 044608 (2014).

[2] C. L. Jiang, B. B. Back, H. Esbensen, J. P. Greene, R. V. F. Janssens, D. J. Henderson, H. Y. Lee, C. J. Lister, M. Notani, R. C. Pardo, N. Patel, K. E. Rehm, D. Seweryniak, B. Shumard, X. Wang, S. Zhu, S. Misicu, P. Collon, and X. D. Tang, Phys. Rev. C **78**, 017601 (2008).

[3] C. L. Jiang, H. Esbensen, K. E. Rehm, B. B. Back, R. V. F. Janssens, J. A. Caggiano, P. Collon, J. Greene, A. M. Heinz, D. J. Henderson, I. Nishinaka, T. O. Pennington, and D. Seweryniak, Phys. Rev. Lett. **89**, 052701 (2002).

[4] N. J. Stone, At. Data Nucl. Data Tables **90**, 75 (2005).

[5] E. Bozek, D. M. De Castro-Rizzo, S. Cavallaro, B. Delaunay, J. Delaunay, H. Dumont, A. D'Onofrio, M. G. Saint-Laurent, L. Sperduto, and F. Terrasi, Nucl. Phys. A **451**, 171 (1986).

[6] G. Colucci, G. Montagnoli, M. Faggian, A. Goasduff, M. Mazzocco, F. Scarlassara, C. Stefanini, E. Strano, M. Urbani, A. M. Stefanini, L. Corradi, E. Fioretto, F. Galtarossa, G. L. Zhang, D. Bourgin, S. Courtin, F. Haas, P. Colović, and S. Szilner, in *Proceedings of the International Nuclear Physics Conference, Adelaide, Australia*, 2016, PoS **281**, 220 (2017).

[7] G. Colucci, G. Montagnoli, A. M. Stefanini, D. Bourgin, P. Čolović, L. Corradi, S. Courtin, M. Faggian, E. Fioretto, F. Galtarossa, A. Goasduff, F. Haas, M. Mazzocco, F. Scarlassara, C. Stefanini, E. Strano, M. Urbani, S. Szilner, and G. L. Zhang, in *Proceedings of the International Conference on Heavy-Ion Collisions at Near-Barrier Energies, Hobart Tasmania, Australia*; EPJ Web Conf. **163**, 00010 (2017).

[8] G. Montagnoli, A. M. Stefanini, C. L. Jiang, H. Esbensen, L. Corradi, S. Courtin, E. Fioretto, A. Goasduff, F. Haas, A. F. Kifle, C. Michelagnoli, D. Montanari, T. Mijatović, K. E. Rehm, R. Silvestri, Pushpendra P. Singh, F. Scarlassara, S. Szilner, X. D. Tang, and C. A. Ur, Phys. Rev. C **85**, 024607 (2012).

[9] J. X. Wei, J. R. Leigh, D. J. Hinde, J. O. Newton, R. C. Lemmon, S. Elfstrom, J. X. Chen, and N. Rowley, Phys. Rev. Lett. **67**, 3368 (1991).

[10] A. M. Stefanini, D. Ackermann, L. Corradi, D. R. Napoli, C. Petrache, P. Spolaore, P. Bednarczyk, H. Q. Zhang, S. Beghini, G. Montagnoli, L. Mueller, F. Scarlassara, G. F. Segato, F. Soramel, and N. Rowley, Phys. Rev. Lett. **74**, 864 (1995).

[11] Ö. Akyüz and Å. Winther, in *Nuclear Structure and Heavy-Ion Physics, Proc. Int. School of Physics "Enrico Fermi", Course LXXVII, Varenna*, edited by R. A. Broglia and R. A. Ricci (North Holland, Amsterdam, 1981).

[12] G. Montagnoli, A. M. Stefanini, H. Esbensen, L. Corradi, S. Courtin, E. Fioretto, J. Grebosz, F. Haas, H. M. Jia, C. L. Jiang, M. Mazzocco, C. Michelagnoli, T. Mijatović, D. Montanari, C. Parascandolo, F. Scarlassara, E. Strano, S. Szilner, and D. Torresi, Phys. Lett. B **746**, 300 (2015).

[13] Ş. Mişicu and H. Esbensen, Phys. Rev. C **75**, 034606 (2007).

[14] H. Esbensen, Phys. Rev. C **85**, 064611 (2012).

[15] I. Angeli, At. Data Nucl. Data Tables **87**, 185 (2004).

[16] S. Gary and C. Volant, Phys. Rev. C **25**, 1877 (1982).